Negatively charged and dark excitons in CsPbBr3 perovskite nanocrystals revealed by high magnetic fields

Damien Canneson, Elena V. Shornikova, Dmitri R. Yakovlev, Tobias Rogge, Anatolie Mitioglu, Mariana V. Ballottin, Peter C. M. Christianen, Emmanuel Lhuillier, Manfred Bayer, Louis Biadala

Communication

Negatively charged and dark excitons in CsPbBr3 perovskite nanocrystals revealed by high magnetic fields

Damien Canneson, Elena V. Shornikova, Dmitri R. Yakovlev, Tobias Rogge, Anatolie A. Mitioglu, Mariana V. Ballottin, Peter C. M. Christianen, Emmanuel Lhuillier, Manfred Bayer, and Louis Biadala

Nano Lett., **Just Accepted Manuscript** • DOI: 10.1021/acs.nanolett.7b02827 • Publication Date (Web): 18 Aug 2017

Negatively charged and dark excitons in $CsPbBr_3$ perovskite nanocrystals revealed by high magnetic fields

Damien Canneson,[†] Elena V. Shornikova,[†,‡] Dmitri R. Yakovlev,[†,¶] Tobias Rogge,[†] Anatolie A. Mitioglu,[§] Mariana V. Ballottin,[§] Peter C. M. Christianen,[§] Emmanuel Lhuillier,[‖] Manfred Bayer,[†,¶] and Louis Biadala*[⊥]

†*Experimentelle Physik 2, Technische Universität Dortmund, 44227 Dortmund, Germany*

‡*Rzhanov Institute of Semiconductor Physics, Siberian Branch of Russian Academy of Sciences, 630090 Novosibirsk, Russia*

¶*Ioffe Institute, Russian Academy of Sciences, 194021 St. Petersburg, Russia*

§*High Field Magnet Laboratory (HFML-EMFL),Radboud University, 6525 ED Nijmegen, The Netherlands*

‖*Sorbonne Universités, UPMC Univ Paris 06, CNRS-UMR 7588, Institut des NanoSciences de Paris, 75005 Paris, France*

⊥*Institut d'Électronique, de Microélectronique et de Nanotechnologie, UMR CNRS 8520, Villeneuve d'Ascq, France*

E-mail:

Abstract

The optical properties of colloidal cesium lead halide perovskite ($CsPbBr_3$) nanocrystals are examined by time-resolved and polarization-resolved spectroscopy in high magnetic fields up to 30 T. We unambiguously show that at cryogenic temperatures the

emission is dominated by recombination of negatively charged excitons with radiative decay time of 300 ps. The additional long-lived emission with a decay time of $8-40$ ns, which decay time shortens and relative amplitude increases in high magnetic fields, evidence the presence of a dark exciton. We evaluate g-factors of the bright exciton $g_X = +2.4$, the electron $g_e = +2.18$ and the hole $g_h = -0.22$.

Keywords

Perovskite, $CsPbBr_3$, dark exciton, trion, time-resolved photoluminescence, high magnetic fields

The past few years, colloidal cesium lead halide nanocrystals ($CsPbX_3$, X=Cl, Br, I) have attracted much attention due to their striking and markedly different optical properties[1] compared to standard II-VI (CdSe, CdTe, HgTe) or III-V (InP, InAs) colloidal semiconductor nanocrystals. Perovskite nanocrystals (NCs) possess a defect tolerant band structure, which results in an ensemble quantum yield (QY) up to 90% at room temperature for the core only materials.[1] In CdSe-based NCs high QY was only obtained in heterostructures, namely when the active core material is capped by a protecting shell made of materials with larger band gap and with a few monolayers thickness.[2] The role played by the shell is not straightforward since it can affect the charge carrier confinement and thereby the optical properties.[3,4] The compelling combination of high QY, ease of the chemical synthesis and wide spectral range makes perovskite NCs very attractive for many applications such as photodectectors,[5] single photon emitters,[6,7] gain medium for low threshold lasing,[8–10] or photovoltaics.[11]

In the large variety of perovskite materials, $CsPbX_3$ nanocrystals have attracted most of attention recently since they allow covering the entire visible spectral range by adjusting composition.[1] Among them $CsPbBr_3$ NCs demonstrate superior stability against photoexcitation and oxidation leading to outstanding optical properties.[12] In particular, at cryogenic temperatures and in low excitation regime (less than one exciton photogenerated per NC by a laser pulse) the emission spectrum of a single uncapped $CsPbBr_3$ NC has a single or

multiple sharp lines (< 1 meV linewidth),[6,13,14] similar to those of core/shell CdSe/ZnS NCs.[15] At cryogenic temperatures the recombination dynamics of $CsPbBr_3$ NCs occurs on two markedly different time scales. Most of the photons are emitted within the first 300 ps and only a small fraction within a few ns.[6,16] Note that it is orders of magnitude faster than recombination of dark excitons in II-VI and III-V colloidal nanostructures with typical decay times of 100 ns to microseconds.[17–21] This raises the question about the exciton fine structure in $CsPbBr_3$ NCs, namely on whether the ground state is dark (spin forbidden) or bright (spin allowed). This is still an open question, which requires experimental efforts.

Temperature dependence of exciton recombination dynamics and magneto-optical properties of emission (line shifts, Zeeman splitting and polarization) are powerful tools to address exciton properties and disclose exciton fine structure in colloidal NCs.[18,22,23] Magneto-optics has not widely been used for perovskite NCs. Only very recently by means of single dot spectroscopy of $CsPbBr_3$ NCs the emission of neutral and charged excitons has been identified[13] an the role of the Rashba effect has been shown.[14] Even for bulk perovskites magneto-optical data are rather limited. $CH_3NH_3PbI_3$ microcrystals were measured in high magnetic fields up to 150 T[24,25] with focus on the exciton binding energy and its dependence on temperature and magnetic field strength. Similar studies have been performed on methylammonium and formamidinium lead tri-halide perovskite semiconductors with chemical structure $APbX_3$, where A=CH_3NH_3 (methylammonium) or $CH(NH_2)_2$ (formamidinium) and X=Cl, Br, I.[26] Magnetic field effects on photocurrent, electroluminescence and photoluminescence were demonstrated for $CH_3NH_3PbI_{3-x}Cl_x$ devices.[27] Theoretical consideration of various magneto-optical properties of excitons and charge carriers in $CH_3NH_3PbI_3$ (g-factors, state mixing, diamagnetic shifts, etc.) can be found in Ref.[28]

In this paper, we investigate recombination and spin dynamics of charged and neutral excitons in ensemble of colloidal $CsPbBr_3$ NCs in temperature range from 4.2 to 300 K and in high magnetic fields up to 30 T. We unveil the presence of the dark exciton state via its long-lasting recombination dynamics shortened by magnetic fields. At cryogenic temperatures the

radiative recombination of negatively charged excitons dominates the PL emission. Electron, hole and exciton g-factors are evaluated from magneto-optical data.

Exciton level structure in perovskite. Electronic structure of $CsPbX_3$ materials was calculated in Ref.,[29] while exciton fine structure in $CsPbX_3$ has not been analyzed theoretically, neither in bulk nor in NCs. Therefore, we relay to a scheme suggested on a base of a group theoretical considerations for 3D crystals of $CH_3NH_3PbX_3$,[30] see Figure 1a. The band structure is somewhat reversed to the one in CdSe-based NCs. In perovskite the conduction band has Γ_4^- (p-like) symmetry and the valence band Γ_1^+ (s-like) symmetry. Spin-orbit interaction, which in CdSe NCs splits states in the valence band, in perovskite acts on the conduction band, splitting it on twofold degenerated Γ_6^- state ($J = 1/2$) and fourfold degenerated Γ_8^- state ($J = 3/2$), J is the total angular momentum. The valence band is then twofold Γ_6^+ state ($J = 1/2$). Exciton is formed from Γ_6^+ and Γ_6^- states and exchange interaction results in the lowest twofold Γ_1^- optically-forbidden dark exciton state ($J = 0$) and in the energetically higher sixfold Γ_4^- optically-allowed bright exciton state ($J = 1$). These two states are relevant to our studies. It is noteworthy that the bright exciton state is further split depending on the crystalline structure.[13] The value of exciton exchange splitting is not known yet for $CsPbX_3$ NCs, and even the order of the bright and dark states is not approved experimentally.

Samples and methods. We investigated $CsPbBr_3$ NCs grown at a temperature of 180°C and dispersed in toluene (for synthesis details see Supporting Information). NCs have an average diameter of 10 nm (see TEM images in Figure 1b), slightly larger than an exciton Bohr diameter of 7 nm.[1] Therefore, excitons experience only a weak quantum confinement. It should be noted that while these NCs are know to crystallize in the cubic phase,[1] a recent report shows that they can exhibit tetragonal and orthorhombic phases at cryogenic temperatures.[13] Absorption and photoluminescence (PL) spectra of this sample measured in solution at room temperature are shown in Figure 1c. Emission has maximum at 2.406 eV and full width at half maximum (FWHM) of 80 meV.

Polarized PL in magnetic field. Circularly polarized photoluminescence spectra measured at magnetic field $B = 15$ T and $T = 4.2$ K are shown in Figure 2a for ensemble of NCs. PL line has maximum at 2.342 eV and a full width at half maximum (FWHM) of 26 meV. PL is polarized in magnetic field (σ^- circularly-polarized component is stronger than σ^+ one) and shows different shifts with increasing magnetic field for the opposite circular polarizations, see Figure 2b. Energy difference between the two components corresponds to the Zeeman splitting of optical transitions $\Delta E_Z = g\mu_B B$, where g is Lande factor and μ_B is the Bohr magneton. It is important to note, that the Zeeman splitting of optical transitions of neutral exciton (X, namely its bright state) and charged excitons are same as they are determined by the sum of the spin splitting in the initial and the final states of the optical transition which is the sum of the electron and the hole splitting independent of the exciton complex. This Zeeman splitting is controlled by an exciton g-factor, which is composed of electron and hole g-factors: $g_X = g_e - g_h$. (We neglect here possible small modifications of g_e and g_h in negatively (T^-) and positively (T^+) charged excitons.) In Figure 2c the Zeeman splitting shows linear dependence on the magnetic field with small deviation in fields exceeding 10 T, which can be fitted with $g = +2.4$. We use in this paper definition of exciton and carrier g-factors and spin schemes in line with Refs. 3,31,33, details are given in Supporting Information. One should distinguish Zeeman splitting of optical transitions from the Zeeman splitting of the initial states of neutral and charged excitons which differs from each other, since they are contributed by g_X for the neutral exciton, by g_h for T^-, and by g_e for T^+, see Figure 2e,f and Supporting Information S3. Typically, the degree of circular polarization (DCP) induced by the magnetic field results from the Zeeman splitting of the initial state since it originates from the thermalization of excitons (or trions) on their Zeeman split levels.[33] It is defined as $P_c = (I^+ - I^-)/(I^+ + I^-)$, where I^+ and I^- are PL intensities in σ^+ and σ^- circular polarizations.

The DCP dependence on the magnetic field is shown in Figure 2d. P_c is negative as the σ^- component is stronger. The DCP is further described by $P_c = P_{sat}[\tau/(\tau +$

$\tau_s)]\tanh(g\mu_B B/2k_B T)$.[33] Here P_{sat} is DCP saturation value, which for isotropic g-factor can be taken as 1, τ is the lifetime of the exciton (trion) and τ_s its spin relaxation time, k_B is Boltzmann constant. $\tau/(\tau+\tau_s)$ is the so-called dynamical factor, which decreases P_c if the spin relaxation does not occur during the lifetime. In case of $\tau_s \ll \tau$ the dynamical factor is equal to 1. T is the temperature of excitons (trions), it is common to take it equal to a bath (lattice) temperature, but under high optical excitation it can exceed the bath temperature, which would decrease DCP. We have checked that DCP is independent of excitation density in range from 2 to 1000 mW/cm^2 (Supporting Information, Figure S1), which allows us to take T equal to the bath temperature of 4.2 K.

In order to be able to evaluate g-factor from $P_c(B)$ dependence one need to know P_{sat}, dynamical factor and T. In our case of isotropic g-factor, $P_{sat} = 1$. We have measured τ_s by time-resolved recombination of polarized PL (see Ref. 33 for method). Dynamics of $P_c(t)$ is shown in inset of Figure 2d. One can see, that the DCP dynamics is faster than the system time-resolution and the most DCP is gained already within 100 ps after the laser pulse. As we will show below, the recombination time at $T = 4.2$ K is $\tau = 300$ ps. Therefore, the dynamical factor in the studied sample is larger than 0.75 (we take it equal to 1 for evaluations). As a result, we end up with $|g| = 0.22$. Note, that for assigning of the g-factor sign, it is necessary to identify the exciton complex that participate in the emission.

In the case of exciton emission, the g-factors evaluated from the Zeeman splitting and $P_c(B)$ should be equal. Their large difference in our experiment attests that the PL is dominated by charged excitons (trions), either negatively or positively charged. As one can see in schemes of Figure 2e,f, Zeeman splitting of trion optical transitions is contributed by both hole (electron) splitting in initial state and electron (hole) splitting in final state for negatively (positively) charged trions, i.e. it is characterized with $g_X = g_e - g_h$. Instead the trion DCP is controlled by the Zeeman splitting of its initial state, i.e. by g_h for negative trion and g_e for positive trion. In depth consideration, which details are given in Supporting Information, allows us to conclude that our experimental situation can be realized only for the

negative trion and for the set of g-factors: $g_e > 0$, $g_h < 0$ and $|g_e| > |g_h|$, which corresponds to the scheme in Figure 2e. Therefore, we can evaluate all g-factors in the studied $CsPbBr_3$ NCs: $g_X = +2.4$, $g_h = -0.22$ and $g_e = +2.18$. Note, that they are comparable with the exciton g-factor in $CsPbBr_3$ NCs[13] and carrier g-factors in $CH_3NH_3PbCl_xI_{3-x}$.[34] The reason for the small hole g-factor, which strongly deviates from 2, is the strong spin-orbit interaction. Such behavior is well known in II-VI and III-V semiconductors,[35,36] where the electron g-factor in the conduction band can be considerably modified. The respective changes are accounted by the Roth-Lax-Zwerdling formulae.[37] Due to inverted band structure in perovskite, the strong spin-orbit modification of the g-factor takes place for the holes states in the valence band.[28] Importantly, the DCP increase with magnetic field for excitons with $g_X = 2.4$ should be ten times faster than what has been measured and shown in Figure 2d. Therefore, we conclude that in our experiment negative trions dominates PL, and the possible contribution of neutral excitons does not exceed 10% of the integral emission. Time-resolved data given below confirm this conclusion.

Interestingly, we observe a shift of the center-of-gravity of the two circularly polarized PL lines (open circles in Figure 2b) as a result of the diamagnetic shift. The shift of the negative trion in magnetic field should generally follow the diamagnetic shift of the neutral exciton. At $B = 15$ T the shift reaches 0.8 meV, which corresponds to a diamagnetic coefficient of 3.3 μeV/T^2. It is in agreement with a few μeV/T^2 estimated in Ref. 13 for $CsPbBr_3$ NCs. Close value of 2.7 μeV/T^2 has been reported for $CH_3NH_3PbI_3$ microcrystals[24] measured in magnetic fields up to 40 T. Some deviation from the B^2 shift can be related to the fact that the trion binding energy can also change in magnetic field, which has been well documented for CdTe- and ZnSe-based quantum wells.[38,39]

Temperature dependence of PL dynamics. Modification of the PL dynamics in wide temperature range between 4.2 and 300 K is shown in Figure 3a. When the temperature is increased up to 300 K, we observe a significant lengthening of the fast component from 300 ps to 5 ns, in agreement with previous reports.[1,16,40] The PL integrated intensity is

about constant in the temperature range from 4.2 to 70 K, in agreement with the picture of trions. As one can see from Figure 3b, most changes take place above 70 K. The PL decay lengthens and the integrated PL intensity decreases as the temperature increases to 300 K. These concomitant observations suggest the thermal activation of trap state, where the trapping/release of charge carriers lengthens the PL decay and reduces the PL intensity.[41]

PL dynamics in magnetic field. Recombination dynamics measured at low temperatures is a useful information for the identification of the exciton states in colloidal NCs.[42,43] In the commonly used case of the ground state formed by the dark exciton, the dynamics has typically fast and long decays. The fast one is due to radiative recombination and energy relaxation of the bright exciton and the long one due to recombination of the dark exciton.[22] External magnetic field mix dark and bright exciton states slowing down the fast decay and accelerating the long one. In contrast, the dynamics of charged excitons having only bright state has only one fast component, which is longer than the bright exciton one as it is contributed only by the radiative recombination.[18,33] The charged exciton dynamics is not sensitive to magnetic field.

Recombination dynamics measured for $CsPbBr_3$ NCs at $T = 4.2$ K in various magnetic fields up to 30 T are shown in Figure 4a. At zero field the fast initial delay with a characteristic time of 300 ps covers three orders of magnitude of the emission decay. The longer contribution is very small in amplitude and is close to the sensitivity level of the experimental setup. With increasing magnetic field no change for the fast decay component happen: the time stays constant and even at 30 T its amplitude covers about two orders of magnitude in the PL intensity decay. While the longer component increases considerably in amplitude, its time-integrated contribution to the PL decay reaches only 20%, see Figure 4b. The decay time of the long component decreases from 36 ns at 10 T to 8 ns at 30 T, see Figure 4c. Note, that the time-integrated PL intensity only slightly increases by less than 10% upon rising the magnetic from 0 to 30 T (inset Figure 4a).

Experimental results on PL dynamics let us conclude that in the studied sample at $T = 4.2$ K emission is dominated by charged excitons with radiative recombination time of 300 ps. This is in full accordance with our conclusion from magneto-optical data measured under *cw* excitation and presented in Figure 2 and with a temperature independency of the PL decay up to 70 K (Figure 3). These results demonstrate the pivotal role of negatively charged excitons in optical properties of ensemble of $CsPbBr_3$ NCs. Note, that this requires that the large part of NCs in ensemble are singly charged with a resident electron, most probably via a photocharging process. Recently, it was shown that at room temperature charged excitons play a dominant role in emission even under weak photoexcitation.[44]

However, the long component can only originate from the neutral excitons emitting from neutral NCs. We can tentatively estimate the quote of the neutral NCs of $10 - 20\%$ of the total number of NCs in the ensemble. It is also in line with our conclusion from Figure 2d. Shortening of the decay time and increase of the amplitude with increasing magnetic field are characteristic features of the spin-forbidden dark exciton state.[42,43] Therefore, we may conclude that the exciton fine structure suggested in Ref. 30 for bulk perovskites $CH_3NH_3PbBr_3$ and $CH_3NH_3PbI_3$ (Figure 1a) is also valid for $CsPbBr_3$ NCs.

In summary, we present detailed study of $CsPbBr_3$ nanocrystals by means of time-resolved and polarization-resolved spectroscopy in high magnetic fields up to 30 T. We show that a combination of the Zeeman splitting of emission line and the degree of its circular polarization provides a convincing way to disclose the origin of the low-temperature photoluminescence. In the studied sample, the emission is dominated by negatively charged excitons (trions), i.e. at low temperatures and under illumination the NCs are predominantly singly-charged by an electron. In ensemble measurements contribution of neutral excitons (i.e. of neutral NCs) does not exceed 10%. Charged excitons recombine within 300 ps. The longer decaying emission of $8 - 40$ ns, which decay time shortens and relative amplitude increases in high magnetic fields, gives direct evidence of the presence of a dark exciton state. We evaluate g-factors of the bright exciton $g_X = +2.4$, electron $g_e = +2.18$ and hole $g_h = -0.22$.

Methods

The sample has been synthesized using the process described in Ref. 7, see Supporting Information for details. The sample was prepared for ensemble measurement by dropcasting the solution of $CsPbBr_3$ perovskite NCs on a glass coverslip. It was excited non-resonantly by a pulsed laser (wavelength 405 nm, pulse duration 100 ps, repetition rate between 100 kHz and 5 MHz) with a weak average power density < 1 W/cm^2 to avoid contributions from radiative recombination of multiexcitons.

Temperature dependence measurements: the sample was mounted in a flow, gas exchange, helium cryostat. The PL signal collected with a 10 cm lens was filtered from the laser by a longpass optical filter and detected by an avalanche photodiode (APD) connected to a conventional time-correlated single-photon counting setup or to a liquid-nitrogen-cooled charge-coupled-device (CCD) after transmission through a 0.55-m spectrometer.

Spin dynamics measurements were performed at $T = 4.2$ K for the sample being in contact with helium exchange gas. External magnetic fields up to 15 T, generated by a superconducting solenoid, were applied in the Faraday geometry, i.e. parallel to the optical axis. The PL signal was dispersed by a 0.55-m spectrometer and detected by a liquid-nitrogen-cooled charge-coupled-device (CCD) or an APD connected to a conventional time-correlated single-photon counting setup. The temporal resolution of our setup is 100 ps.

PL decay in magnetic fields up to 30 T. These measurements were performed in High Magnetic Field Lab, Nijmegen. The NC sample was mounted in a titanium sample holder on top of a three-axis piezo-positioner. The sample stage was placed in a homemade optical probe, made of carbon and titanium to minimize possible displacements at high magnetic fields. Laser light was focused on the sample by a lens (10 mm focal length). The same lens was used to collect the PL emission and direct it to the detection setup (backscattering geometry). The optical probe was mounted inside a liquid helium bath cryostat (4.2 K) inserted in a 50 mm bore Florida-Bitter electromagnet with a maximum *dc* magnetic field strength of 31 T. Experiments were performed in Faraday geometry (light excitation and

detection parallel to the magnetic field direction). For time-resolved PL measurements the excitation was provided by a picosecond pulsed diode-laser operating at 405 nm. The PL signal was detected by an avalanche photodiode connected to a single-photon counter (time-correlated single photon counting).

ASSOCIATED CONTENT

Details of synthesis of $CsPbBr_3$ NCs. Magnetic field dependences of the circular polarization degree measured at various excitation densities (Figure S1). Spin structure of exciton and singlet states of negatively and positively charged trions in magnetic field (Figure S2). Long-living PL dynamics in magnetic fields (Figure S3).

AUTHOR INFORMATION

Corresponding Author

*louis.biadala@isen.iemn.univ-lille1.fr

Notes

The authors declare no competing financial interest.

ACKNOWLEDGEMENTS

The authors are thankful to A.V. Rodina and Al.L. Efros for stimulating discussions. We aknowledge the support from HFML-RU/FOM, a member of the European Magnetic Field Laboratory (EMFL). This work was supported by French state funds managed by the ANR within the Investissements d'Avenir programme under the reference ANR-11-IDEX-0004-02, and more specifically within the framework of the Cluster of Excellence MATISSE led by Sorbonne Universités. We acknowledge the financial support by the Deutsche Forschungsgemeinschaft in the frame of the Sonderforschungsbereich TRR160 (and TRR142) and by the Government of Russia (project number 14.Z50.31.0021, leading scientist M. Bayer).

References

1. Protesescu, L.; Yakunin, S.; Bodnarchuk, M. I.; Krieg, F.; Caputo, R.; Hendon, C. H.; Yang, R. X.; Walsh, A.; Kovalenko, M. V. *Nano Lett.* **2015**, 15, 3692-3696.

2. Hines, M. A.; Guyot-Sionnest, P. *J. Phys. Chem.* **1996**, 100, 468-471.

3. Javaux, C.; Mahler, B.; Dubertret, B.; Shabaev, A.; Rodina, A. V; Efros, A. L.; Yakovlev, D. R.; Liu, F.; Bayer, M.; Camps, G.; et al. *Nat. Nanotechnol.* **2013**, 8, 206-212.

4. Christodoulou, S.; Rajadell, F.; Casu, A.; Vaccaro, G.; Grim, J. Q.; Genovese, A.; Manna, L.; Climente, J. I.; Meinardi, F.; Rainó, G.; et al. *Nat. Commun.* **2015**, 6, 7905.

5. Ramasamy, P.; Lim, D.-H.; Kim, B.; Lee, S.-H.; Lee, M.-S.; Lee, J.-S. *Chem. Commun.* **2016**, 52, 2067-2070.

6. Rainó, G.; Nedelcu, G.; Protesescu, L.; Bodnarchuk, M. I.; Kovalenko, M. V; Mahrt, R. F.; Stöferle, T. *ACS Nano* **2016**, 10, 2485-2490.

7. Park, Y.-S.; Guo, S.; Makarov, N. S.; Klimov, V. I. *ACS Nano* **2015**, 9, 10386-10393.

8. Yakunin, S.; Protesescu, L.; Krieg, F.; Bodnarchuk, M. I.; Nedelcu, G.; Humer, M.; De Luca, G.; Fiebig, M.; Heiss, W.; Kovalenko, M. V. *Nat. Commun.* **2015**, 6, 8056.

9. Xu, Y.; Chen, Q.; Zhang, C.; Wang, R.; Wu, H.; Zhang, X.; Xing, G.; Yu, W. W.; Wang, X.; Zhang, Y.; et al. *J. Am. Chem. Soc.* **2016**, 138, 3761-3768.

10. Eaton, S. W.; Lai, M.; Gibson, N. A.; Wong, A. B.; Dou, L.; Ma, J.; Wang, L.-W.; Leone, S. R.; Yang, P.; Duan, X.; et al. *PNAS* **2016**, 113, 1993-1998.

11. Sutton R. J.; Eperon G. E.; Miranda L.; Parrott E. S.; Kamino B. A.; Patel J. B.; Horantner M. T.; Johnston M. B.; Haghighirad A. A.; Moore D. T.; Snaith H. J. *Adv. Energy Mater.* **2016**, 6, 1502458.

12. ten Brinck, S.; Infante, I. *ACS Energy Lett.* **2016**, 1, 1266-1272.

13. Fu, M.; Tamarat, P.; Huang, H.; Even, J.; Rogach, A. L.; Lounis, B. *Nano Letters* **2017**, 17, 28952901.

14. Isarov, M.; Tan, L. Z.; Bodnarchuk, M. I.; Kovalenko, M. V.; Rappe, A.M.; Lifshitz, E. *NANO Lett.* **2017**, DOI:10.1021/acs.nanolett.7b02248.

15. Biadala, L.; Louyer, Y.; Tamarat, P.; Lounis, B. *Phys. Rev. Lett.* **2009**, 103, 37404.

16. Hu, F.; Zhang, H.; Sun, C.; Yin, C.; Lv, B.; Zhang, C.; Yu, W. W.; Wang, X.; Zhang, Y.; Xiao, M. *ACS Nano* **2015**, 9, 12410-12416.

17. Biadala, L.; Siebers, B.; Beyazit, Y.; Tessier, M. D.; Dupont, D.; Hens, Z.; Yakovlev, D. R.; Bayer, M. *ACS Nano* **2016**, 10, 3356-3364.

18. Labeau, O.; Tamarat, P.; Lounis, B. *Phys. Rev. Lett.* **2003**, 90, 257404.

19. de Mello Donegá, C.; Bode, M.; Meijerink, A. *Phys. Rev. B* **2006**, 74, 85320.

20. Biadala, L.; Siebers, B.; Gomes, R.; Hens, Z.; Yakovlev, D. R.; Bayer, M. *J. Phys. Chem. C* **2014**, 118, 22309-22316.

21. Cassette, E.; Mahler, B.; Guigner, J.-M.; Patriarche, G.; Dubertret, B.; Pons, T. *ACS Nano* **2012**, 6, 6741-6750.

22. Rodina, A. V; Efros, Al. L. *Phys. Rev. B* **2016**, 93, 155427.

23. Furis, M.; Hollingsworth, J. A.; Klimov, V. I.; Crooker, S. A. *J. Phys. Chem. B* **2005**, 109, 15332-15338.

24. Hirasawa, M.; Ishihara, I.; Goto, T.; Uchida, K.; Miura, N. *Physica B* **1994**, 201, 427-430.

25. Miyata, A.; Mitioglu, A.; Plochocka, P.; Portugall, O.; Wang, J. T.-W.; Stranks, S. D.; Snaith, H. J.; Nicholas, R. J. *Nature Physics* **2015**, 11, 582-587.

26. Galkowski, K.; Mitioglu, A.; Miyata, A.; Plochocka, P.; Portugall, O.; Eperon, G. E.; Wang, J. T.-W.; Stergiopoulos, T.; Stranks, S. D.; Snaith, H. J.; Nicholas, R. J. *Energy Environ. Sci.* **2016**, 9, 962-970.

27. Zhang, C.; Sun, D.; Sheng, C.-X.; Zhai, Y. X.; Mielczarek, K.; Zakhidov, A.; Vardeny, Z. V. *Nature Physics* **2015**, 11, 427-434.

28. Yu, Z. G. *Scientific Reports* **2016**, 6:28756, DOI: 10.1038/srep28576.

29. Heidrich, K.; Schäfer, W.; Schreiber, M.; Söchtig, J.; Trendel, G.; Treusch, J. *Phys. Rev. B* **1981**, 24, 5642-5649.

30. Tanaka, K.; Takahashi, T.; Ban, T.; Kondo, T.; Uchida, K.; Miura, N. *Solid State Commun.* **2003**, 127, 619-623.

31. Efros, Al. L. in Semiconductor and Metal Nanocrystals: Synthesis and Electronic and Optical Properties, edited by Klimov, V. I. (Dekker, New York, 2003), Chap. 3, pp. 103141.

32. Efros, Al. L.; Rosen, M.; Kuno, M.; Nirmal, M.; Norris, D. J.; Bawendi, M. *Phys. Rev. B* **1996**, 54, 4843-4856.

33. Liu, F.; Biadala, L.; Rodina, A. V.; Yakovlev, D. R.; Dunker, D.; Javaux, C.; Hermier, J.-P.; Efros, A. L.; Dubertret, B.; Bayer, M. *Phys. Rev. B* **2013**, 88, 35302.

34. Odenthal, P.; Talmadge, W.; Gundlach, N.; Wang, R.; Zhang,C.; Sun, D.; Yu, Z.-G.; Vardeny, Z.V.; Li, Y. S. *Nature Physics* **2017** DOI: 10.1038/NPHYS4145

35. Sirenko, A. A.; Ruf, T.; Cardona, M.; Yakovlev, D. R.; Ossau, W.; Waag, A.; Landwehr, G. *Phys. Rev. B* **1997**, 56, 2114-2119.

36. Yugova, I. A.; Greilich, A.; Yakovlev, D. R.; Kiselev, A. A.; Bayer, M.; Petrov, V. V.; Dolgikh, Yu. K.; Reuter, D.; Wieck, A. D. *Phys. Rev. B* **2007**, 75, 245302.

37. Roth, L. M.; Lax, B.; Zwerdling, S. *Phys. Rev.* **1959**, 114, 90-104.

38. Bartsch, G.; Gerbracht, M.; Yakovlev, D. R.; Blokland, J. H.; Christianen, P. C. M.; Zhukov, E. A.; Dzyubenko, A. B.; Karczewski, G.; Wojtowicz, T.; Kossut, J.; Maan, J. C.; Bayer, M. *Phys. Rev. B* **2011**, 83, 235317.

39. Astakhov, G. V.; Yakovlev, D. R.; Kochereshko, V. P.; Ossau, W.; Faschinger, W.; Puls, J.; Henneberger, F.; Crooker, S. A.; McCulloch, Q.; Wolverson, D.; Gippius, N. A.; Waag, A. *Phys. Rev. B* **2002**, 65, 165335.

40. Makarov, N. S.; Guo, S.; Isaienko, O.; Liu, W.; Robel, I.; Klimov, V. I. *Nano Lett.* **2016**, 16, 2349-2362.

41. Jones, M.; Lo, S. S.; Scholes, G. D. *J. Phys. Chem. C* **2009**, 113, 18632

42. Nirmal, M.; Norris, D. J.; Kuno, M.; Bawendi, M. G.; Efros, Al. L.; Rosen, M. *Phys. Rev. Lett.* **1995**, 75, 3728-3731.

43. Biadala, L.; Louyer, Y.; Tamarat, P.; Lounis, B. *Phys. Rev. Lett.* **2010**, 105, 157402.

44. Yarita, N.; Tahara, H.; Ihara, T.; Kawawaki, T.; Sato, R.; Saruyama, M.; Teranishi, T.; Kanemitsu, Y. *J. Phys. Chem. Lett.* **2017**, 8, 1413-1418.

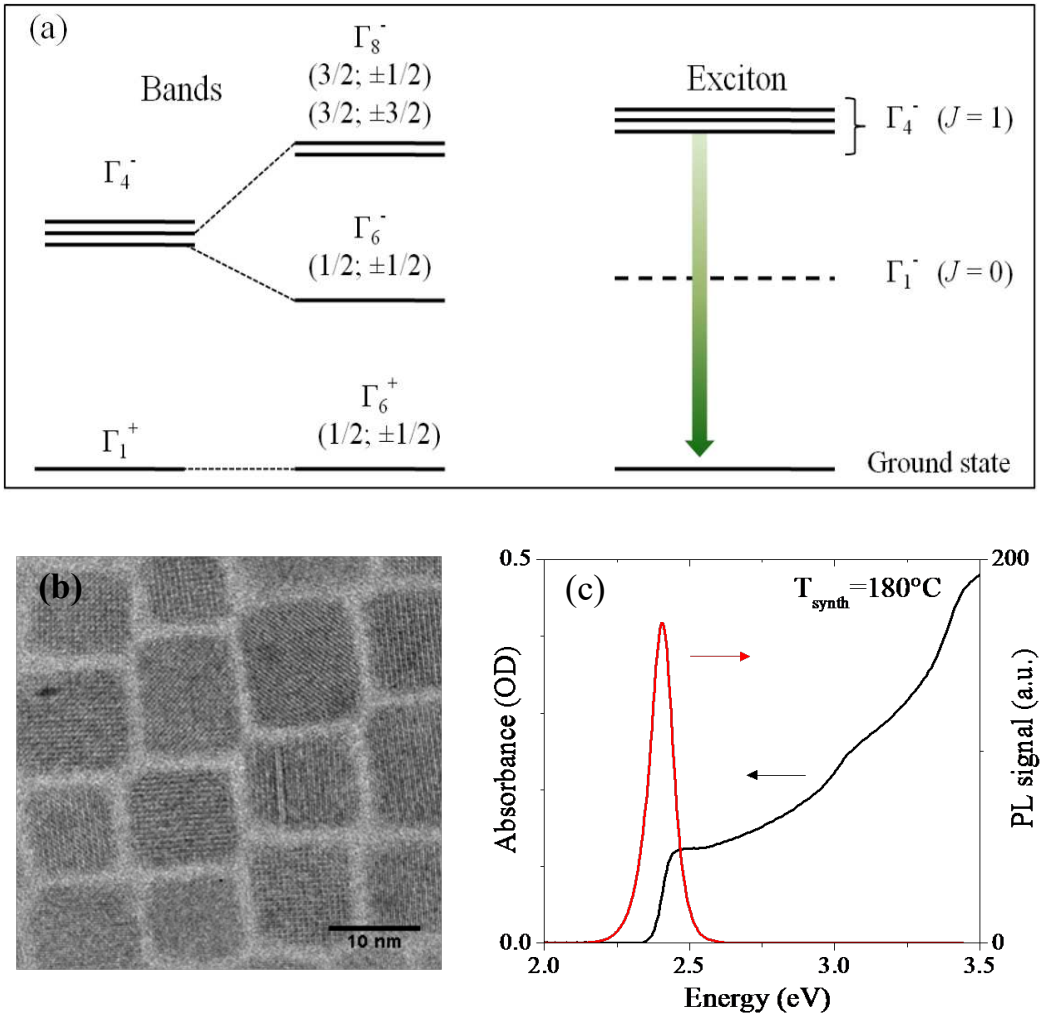

Figure 1: (a) Schematic energy diagrams adopted from Ref.[30] Left side is for conduction and valence bands with Γ_4^- and Γ_1^+ symmetry, respectively. Due to spin-orbit interaction the conduction band splits into Γ_8^- and Γ_6^- states and the valence band transforms as Γ_6^+. Right side shows lowest dark (Γ_1^-, $J = 0$) and bright (Γ_4^-, $J = 1$) exciton states. Ground state here is the state of unexcited crystal. (b) Transmission electron microscopy (TEM) image of the sample grown at 180°C dispersed in toluene. (c) Absorption and photoluminescence spectra of this sample measured in solution at room temperature.

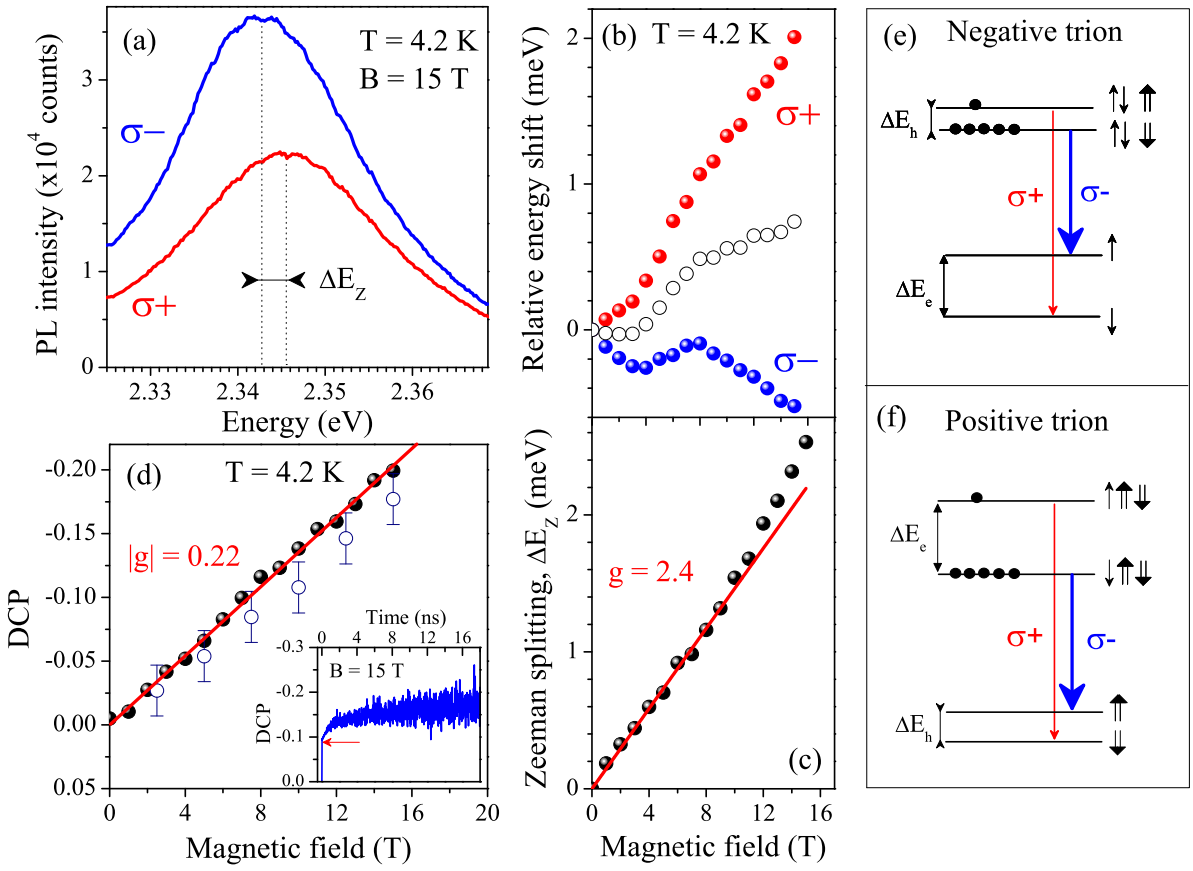

Figure 2: (a) Time-integrated polarization-resolved PL spectra of $CsPbBr_3$ NCs at $B = 15$ T and $T = 4.2$ K. The spectra are split by the Zeeman splitting, ΔE_Z. (b) Magnetic field dependence of the relative spectral positions of σ^- (blue circles) and σ^+ (red circles) components. Open circles show shift of the center-of-gravity of the two polarized components, corresponding to the exciton shift without contribution of the Zeeman splitting. (c) Zeeman splitting of emission line. Red line is a linear fit with $|g| = 2.4$. (d) Magnetic field dependence of the time-integrated DCP (black dots) and saturated DCP (open blue). Both dependences are fit with a g-factor of 0.22 (red line). Inset: Time-resolved DCP at 15 T displaying ultrafast spin dynamics. Arrow indicates the polarization level at initial time. Schematic presentation of the spin level structure and the optical transitions between these levels for (e) negative trions and (f) positive trion in an external magnetic field. Thin and large black arrows indicate electron and hole spins, respectively. Polarized optical transitions are shown by red (σ^+) and blue (σ^-) arrows. The more intense emission, shown by thicker arrow, comes from the lowest in energy trion state. Here we consider $g_e > 0$, $g_h < 0$ and $|g_e| > |g_h|$.

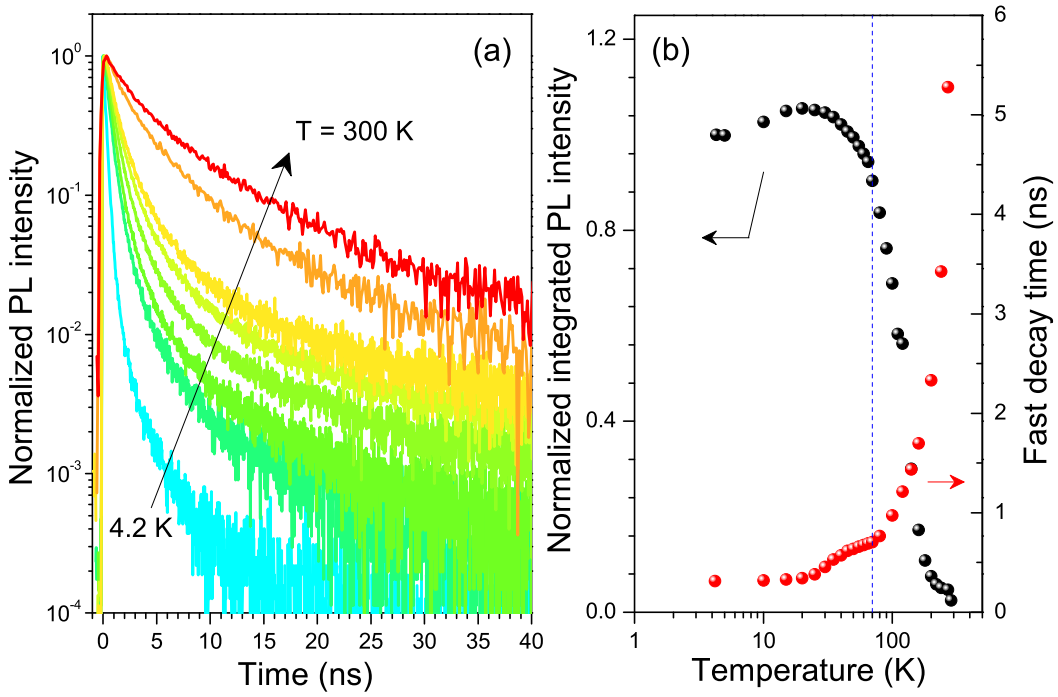

Figure 3: (a) PL decays at various temperatures between 4.2 K and 300 K of colloidal $CsPbBr_3$ NCs. (b) Temperature dependence of the integrated PL intensity (black) and the decay time of the short component of the PL decay (red).

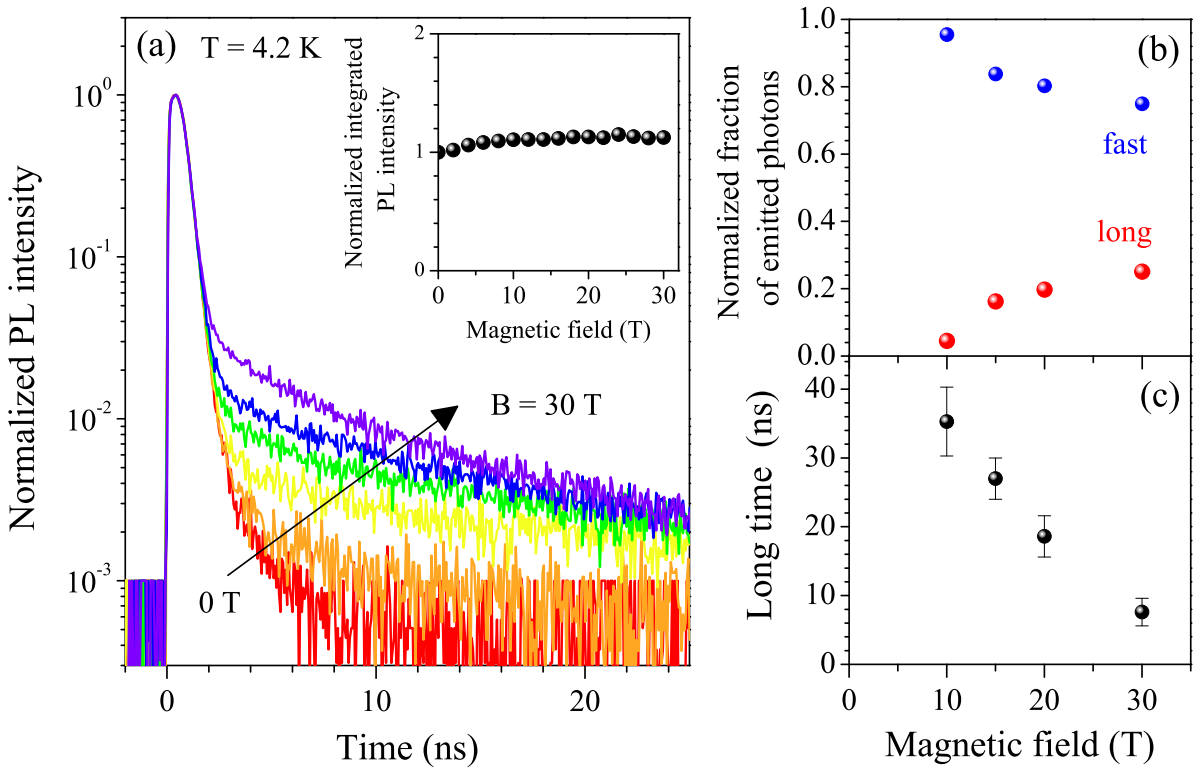

Figure 4: (a) Unpolarized PL decay at $B =$ 0, 5, 10, 15, 20 and 30 T showing the magnetic field activation of the long component. Inset: normalized integrated PL intensity. Magnetic field dependences of (b) normalized fraction of emitted photons with a long (red) and fast (blue) time. (c) Magnetic field dependence of decay time of long component. Note that the weak intensity of the long component prevent reliable fitting below $B = 10$ T.